New Journal of Physics
The open–access journal for physics

Temperature insensitivity of the spin-polarization in Co_2MnSi films on GaAs (001)

W R Branford[1,2], L J Singh[3], Z H Barber[3], A Kohn[4], A K Petford-Long[4], W Van Roy[5], F Magnus[1], K Morrison[1], S K Clowes[1], Y V Bugoslavsky[1] and L F Cohen[1]

[1] Blackett Laboratory, Imperial College, Prince Consort Rd, London, SW7 2BZ, UK
[2] Department of Chemistry, UCL, Gordon Street, London WC1H OAJ, UK
[3] Department of Materials Science and Metallurgy, University of Cambridge, Pembroke Street, Cambridge CB2 3QZ, UK
[4] Department of Materials, University of Oxford, Parks Road, Oxford OX1 3PH, UK
[5] IMEC, Kapeldreef 75, B-3001 Leuven, Belgium
E-mail: w.branford@imperial.ac.uk

New Journal of Physics **9** (2007) 42
Received 6 October 2006
Published 28 February 2007
Online at http://www.njp.org/
doi:10.1088/1367-2630/9/2/042

Abstract. The Heusler alloys Co_2MnSi and NiMnSb are predicted to be 100% spin-polarized and are leading candidate materials for spin-injection and detection in hybrid spintronic devices. Co_2MnSi is lattice matched with GaAs, whereas NiMnSb is strongly mismatched to GaAs. Here, we study the temperature and thickness dependence of the anomalous Hall (AH) effect in a series of textured, predominantly (001) oriented, sputter deposited Co_2MnSi thin films on GaAs, and compare the behaviour to that of a molecular beam epitaxy (MBE) grown NiMnSb film on GaAs (001) with low antisite disorder. We show that the Co_2MnSi films have temperature independent AH conductivity, even for the thinnest films with strongly temperature dependent saturation magnetization. We discuss whether a temperature insensitive AH conductivity necessarily indicates that the spin-polarization of charge carriers is also temperature independent.

PII: S1367-2630(07)34448-0

Co_2MnSi and NiMnSb are two of the most promising spintronic injector/detector materials. Co_2MnSi is a full Heusler alloy, and NiMnSb is a half-Heusler alloy. Both crystallize in the $L2_1$ structure (space group Fm3m), and have been predicted to be half metallic ferromagnets [1] with a large energy gap in the minority band ($\sim$0.4 eV for Co_2MnSi, $\sim$0.5 eV for NiMnSb [2]). Their respective Curie temperatures are 985 K [3, 4] and 730 K [5].

Heuslers can suffer from antisite disorder [6] because of similar atomic radii of the metal ions. However, calculations have indicated that in Co_2MnSi the bare band structure spin-polarization, P_0 (the difference of the density of states at the Fermi energy for spin-up and spin-down carriers) is robust to the presence of antisite defects. This is in marked contrast to many other Heusler alloys, including NiMnSb [7]–[9].

The anomalous Hall (AH) resistivity is well studied, particularly for ferromagnetic metals [10]. Empirically, it can be described as being proportional to the magnetization of a sample, giving a total Hall resistivity of $\rho_{xy} = R_O B + R_S \mu_0 M$, where R_O and R_S are known respectively as the ordinary and AH coefficients and $\mu_0 M$ is the magnetization. Theory suggests that there is a much more general phenomenon, known as the spin Hall effect [11]–[14]. The spin Hall effect describes a transverse deflection of current carriers, which can arise from either intrinsic or extrinsic processes in the presence of spin-orbit coupling, and results in an off-diagonal carrier velocity which is proportional to $(\lambda \cdot \mathbf{E} \times \mathbf{s})$ where $\mathbf{s}$ is the carrier spin-vector, $\mathbf{E}$ is the electric field vector and λ is the spin-orbit coupling constant. The cross product results in equal and opposite terms for spin-up and spin-down carriers and produces a spatial separation of spin-currents [13, 15]. This results in an AH charge-current, J_{AH}, proportional to $(\lambda \cdot \mathbf{E} \times \mathbf{S})$ where $\mathbf{S}$ is the total spin-vector of the charge carriers, which is related to P_t. In unpolarized systems $J_{AH} = 0$ and there is pure spin-separation, whereas in naturally polarized systems there is concomitant charge separation which results in the readily observable AH voltage. The intrinsic AH current density has been defined [16, 17] as $J_{AH} = 2ne^2\lambda \mathbf{E} \times \mathbf{S}$ where n and e are the density and charge of the carriers, respectively. In the mixed or extrinsic regime, the degree of asymmetric (or spin-orbit) and symmetry preserving (or symmetric) scattering within a sample also plays a role in the magnitude of the total AH resistivity measured [18]. Historically, the purely quantum-mechanical intrinsic effect has been described as *side-jump* scattering [16, 19] and this has added to the confusion about the mechanism of the AH effect. In this description the AH resistivity was described as two components, *skew* and *side-jump* terms which are linearly and quadratically dependent on the resistivity, respectively [20]. However, recently it was shown [18] that the *skew* scattering (extrinsic) mechanism alone could result in a mixed linear and quadratic dependence, depending on the relative contributions of symmetric and asymmetric scattering in the material. Hence, we can conclude that it is rather difficult in practice to differentiate between intrinsic and extrinsic mechanisms purely from the dependence of the anomalous Hall term (AHT) on the resistivity.

When evaluating ferromagnetic materials for ferromagnet–semiconductor hybrid devices, the transport spin-polarization, P_t, which can be dramatically different to P_0 [21], is one of the critical parameters that needs to be established. Point contact Andreev reflection (PCAR) spectroscopy can be used, but characterizes the near surface properties only and the information is restricted to low temperatures. Previously, we demonstrated that Co_2MnSi films on sapphire [22, 23] and GaAs [24] have a spin-polarization of 55%, significantly higher than other elemental and alloy-metal ferromagnets, and a P_t of 89% has recently been claimed after annealing at 450 °C [25]. However, recent measurements on Co_2MnSi magnetic tunnel junctions [24] and Co_2MnGe spin-polarized light-emitting diodes (spin-LEDs) [26] have shown a significant deterioration of

the tunnel current spin-polarization with increasing temperature. In the light of these results, it is important to search for other complementary techniques that will measure bulk properties. The AH resistivity is attractive because of its simplicity as a method and it is relatively straightforward to study film properties as a function of thickness and temperature. For example, the study comparing dilute magnetic semiconductors, itinerant ferromagnets and doped Kondo insulators has shown that plotting the AH conductivity is a useful way to classify magnetic systems [27].

The AHT can be used as a gauge of variation of film properties with thickness and temperature but not as an absolute determinant of transport spin-polarization. The combination of AHT from base temperature to room temperature with base temperature PCAR measurement of the polarization [21] appears the best available indication of the room temperature spin transport in ferromagnetic metals.

Previously [28], we demonstrated that in thin films of off-stoichiometric NiMnSb on Si (001) the Hall transport properties varied dramatically as a function of temperature and thickness, indicating very poor performance as a spintronic injector material. Thickness, orientation and surface termination have been predicted [29] to play an important role in the transport spin-polarization of Heusler alloys. Here, we investigate the thickness and temperature dependence of the longitudinal (ρ_{xx}) and Hall (ρ_{xy}) electrical resistivities in highly (001) aligned Co_2MnSi films on lattice-matched GaAs (001). We compare the AHT in Co_2MnSi:GaAs (001) to epitaxial NiMnSb:GaAs (001) grown by molecular beam epitaxy (MBE).

The MBE growth of the 330 nm NiMnSb:GaAs (001) film is described elsewhere [30], the substrate temperature was 300 °C and the Sb/Ni flux ratio was ten. There is no reaction zone in this film [30]. With reference to the sputtered Co_2MnSi films, we note that a Mn_2As interface layer was observed in MBE NiMnSb films grown with a lower antimony flux [30]. The film was shown to have a low level of antisite defects ($\leqslant 4\%$) by nuclear magnetic resonance techniques [31]. The lattice mismatch is 4.4%.

Thin films of Co_2MnSi, with thicknesses of 14, 37, 130 and 260 nm, were grown from three elemental dc magnetron sputtering targets onto GaAs (001) substrates at 374 °C, positioned directly below the targets on a Ta strip heater. The geometry of the set-up is described elsewhere [22]. The x-ray diffraction (XRD) patterns of the Co_2MnSi films are consistent with single-phase highly textured Co_2MnSi, following the orientation of the lattice matched GaAs (001), with a lattice parameter of 5.63 ± 0.01 Å, compared to 5.6521 ± 0.0001 Å for the bulk [32]. No impurity phases were detected in the XRD.

The composition, morphology and thickness of the films was studied with a transmission electron microscope (TEM) [24, 23]. Figure 1 shows TEM bright field images of cross-section of the 14 nm (a) and 260 nm (b) thick Co_2MnSi films, the zone axis is (110). Reaction zones are visible at the Co_2MnSi:GaAs interface in all films, in the thinner layers (up to ∼130 nm) the reaction zones show faceting down into the substrate, approximately along the (111) direction, while in the thicker films the reaction zone appears more continuous. Energy-filtered TEM composition mapping using the L_3 edges [33] shows that the reaction zone is indistinguishable from the rest of the GaAs substrate when mapping arsenic concentration, but gallium is deficient, compared to GaAs. Manganese mapping shows that it is present, and cobalt could not be detected in the reaction zone. However, specific crystalline impurity phases, e.g., MnAs, Mn_2As were not observed in the TEM or the XRD. We note that the volume of the reaction zone approaches that of the 14 nm film Heusler layer, and is well within the resolution of our structural characterization to a crystalline single phase. Thus, we conclude that the reaction zone is either Mn-doped GaAs or a nanocrystalline or amorphous mixture of GaAs and a Mn–As compound, such as MnAs or Mn_2As.

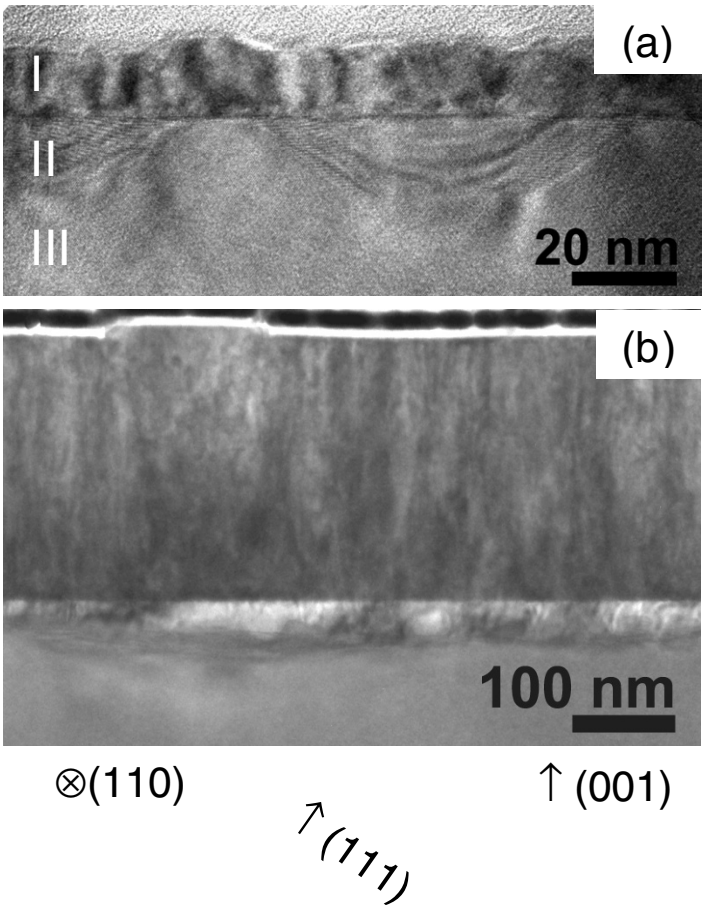

Figure 1. TEM bright field images of cross-section Co_2MnSi film deposited on GaAs (001) substrate. Zone axis is (110). Regions labelled as follows: I: Co_2MnSi film, II: reaction zone III: GaAs substrate.

Magnetotransport data were collected in a square geometry by the van der Pauw method. The pure Hall signal was separated from the magnetoresistive contribution by virtue of their different symmetries with respect to the inversion of the magnetic field. The field dependence of the magnetization of the films was measured at the same temperatures and in the same geometry (field perpendicular to the film surface) as the Hall measurements, in an Oxford Instruments vibrating sample magnetometer. In this geometry, the magnetic anisotropy of the films is dominated by the shape anisotropy.

The Hall resistivity was measured for all the films at selected temperatures between 10 K and 290 K, the data for the 260 nm Co_2MnSi film, which is typical of all the Co_2MnSi films, are shown in figure 2 together with the 330 nm NiMnSb film. An iterative procedure was used to fit the measured Hall resistivity to the expression $\rho_{xy} = R_O B + R_S \mu_0 M$, using independently measured magnetization, which was measured at the same temperature and in the same geometry (with field perpendicular to film surface). With this field orientation, the demagnetization factor (N) is unity, hence the flux density, $B = \mu_0[H + (1 - N)M] = \mu_0 H$, where H is the applied magnetic field in A m^{-1}.

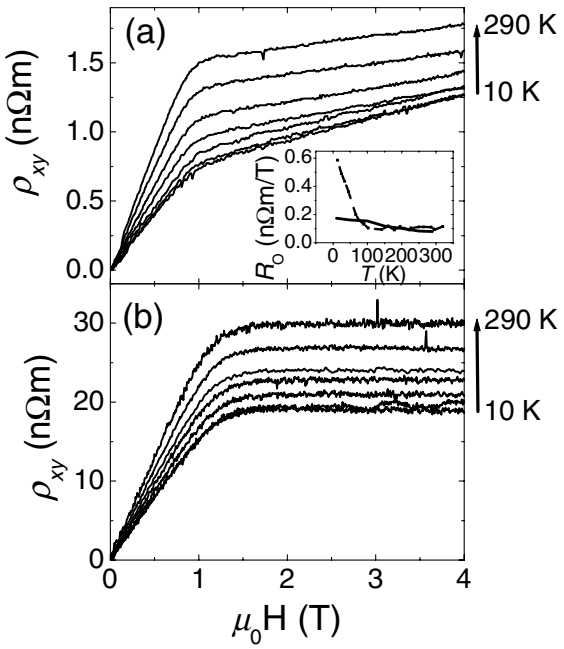

Figure 2. Hall resistivity versus field at 10, 50, 100, 150, 200, 250 and 290 K for (a) 330 nm NiMnSb film and for (b) 260 nm Co_2MnSi film. Inset: ordinary Hall constant versus temperature for NiMnSb film (solid line) and bulk data taken from Otto *et al* [20].

One can immediately see from the raw data shown in figure 2 that there are differences between the Co_2MnSi and the NiMnSb films. Both the magnitude of the Hall signal and the temperature dependence are very different between the films. In particular, it is clear from the raw data that R_S is approximately an order of magnitude larger in Co_2MnSi than NiMnSb, whereas ρ_{xx} is only a factor of between two and four larger, depending on temperature and R_O, the ordinary Hall component, is immeasurably small in Co_2MnSi (the high field part of the curve is effectively completely flat), whereas the high field slope of NiMnSb clearly changes with temperature. In the inset to figure 2(a) we compare the temperature dependence of R_O of the MBE grown film to previous bulk measurements by Otto *et al* [34]. We do not observe the sharp increase below 100 K observed in the bulk, but above 100 K the data are in good agreement with $R_O \sim 0.1\,\mathrm{n\Omega\,m\,T^{-1}}$, indicating that there is no significant change in the quantity or sign of the dominant carriers. In contrast, we previously used this method to show [35] that in polycrystalline NiMnSb films grown on Si, both the quantity and charge of the dominant carriers varied dramatically with temperature and thickness. Using a single carrier model, one could obtain carrier concentration and mobility from the Hall coefficient for NiMnSb, and a lower bound to the concentration for Co_2MnSi, however, it is known that the Heuslers have complex Fermi surfaces, with both hole-like and electron-like regions, and so this is not appropriate here. For the Co_2MnSi films $R_O \ll R_S$ and the high-field magnetic susceptibility of the films could not be accurately determined, so R_O could not be precisely determined from the fitting procedure.

The temperature dependence of the magnetotransport parameters of all the Co_2MnSi and NiMnSb films up to room temperature is shown in figure 3, and absolute values of the

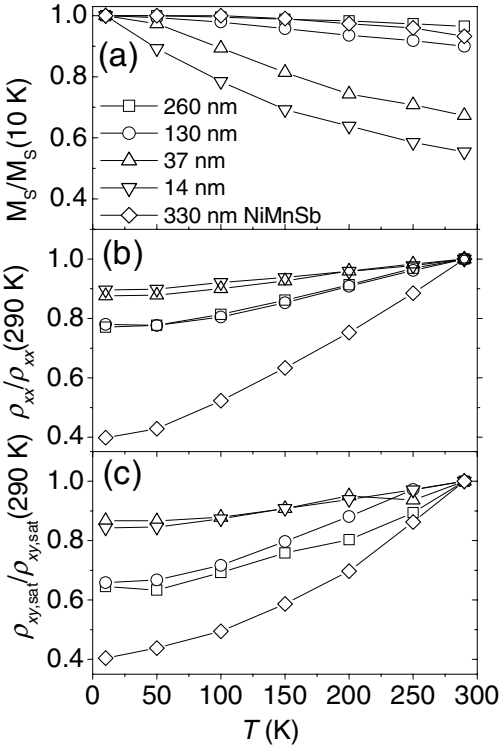

Figure 3. (a) Normalized saturation magnetization versus temperature of the Co_2MnSi and NiMnSb films; (b) normalized longitudinal resistivity versus temperature. Symbol shapes are as in figure 3(a). (c) Normalized saturation Hall resistivity. Symbol shapes are as in figure 3(a).

relevant parameters are given in table 1. Figure 3(a) shows the saturation magnetization, the 260 nm film has magnetic properties similar to that of the stoichiometric bulk material ($T_C = 985\,K$)[3] with $M_S(300\,K)/M_S(5\,K) = 0.97$, whereas it is clear that T_C is reduced for the 14, 37 and 130 nm films. This is consistent with increasingly significant loss of Mn from the Heusler phase to the reaction layer as the films become thinner. The observed behaviour could also be explained by a low Curie temperature ferromagnetic impurity phase forming in the reaction zone. The most likely candidate impurity, Mn_2As [30], is antiferromagnetic, but metallic ferromagnetic MnAs ($T_C = 313\,K$) and dilute ferromagnetic semiconductor Mn-doped GaAs ($T_C =$ up to 140 K) are plausible phases. However, $M_S(300\,K)/M_S(5\,K) = 0.55$ for the 14 nm film, and for this to be caused by impurity phases would require a volume of MnAs approximately equal to the volume of the film, or a volume of Mn-doped GaAs more than an order of magnitude greater than that of the film. Sufficient quantities of MnAs to cause the different temperature dependence of the saturation magnetization cannot be ruled out.

The resistivity (ρ_{xx}) and saturation AH resistivity ($\rho_{xy,sat}$) are compared in figures 3(b) and (c) respectively. The residual resistivity (table 1) of the NiMnSb film is small and the temperature dependence of (ρ_{xx}) is significant, the resistivity ratio (300 K/10 K) is 2.5, so by room temperature thermally activated processes are contributing the majority of the scattering. In contrast, in the thick Co_2MnSi films, the residual resistivity much larger and the resistivity ratio is only 1.3, so temperature independent (defect) scattering dominates all the way up to

Table 1. Magnetotransport parameters for Co_2MnSi:GaAs films and 330 nm NiMnSb:GaAs film. The reaction zone thickness was determined according to the typical maximum intrusion depths of the reaction zones, and the errors represent approximately minimum and maximum depth of observed reaction zones. Composition was measured by energy-dispersive spectroscopy using a small electron probe (∼1 nm in diameter).

	M_S(5 K) (μ_B/f.u.)	M_S(300 K)/ M_S (5 K)	ρ_{xx}(10 K) (Ωm)	ρ_{xx}(300 K) (Ωm)	R(300 K)/ R(10 K)	Thickness and composition of interface diffusion layer
14 nm Co_2MnSi	3.56	0.55	1.33×10^{-6}	1.49×10^{-6}	1.12	Mn, As rich—graded composition 13.5 ± 2 nm
37 nm Co_2MnSi	3.55	0.67	1.28×10^{-6}	1.55×10^{-6}	1.21	Composition not measured 12.8 ± 3.5 nm
130 nm Co_2MnSi	4.19	0.90	5.30×10^{-7}	6.80×10^{-7}	1.28	Mn:As 1:1 25 ± 9 nm
260 nm Co_2MnSi	3.75	0.97	5.56×10^{-7}	7.21×10^{-7}	1.30	Mn:As 60:40 49 ± 16 nm
330 nm NiMnSb	3.22	0.93	1.26×10^{-7}	3.17×10^{-7}	2.50	Not measured

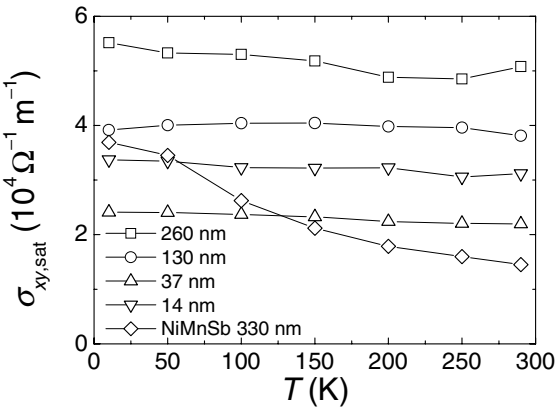

Figure 4. Saturation anomalous Hall (AH) conductivity versus temperature for Co_2MnSi:GaAs and NiMnSb:GaAs films.

room temperature. The residual resistivity of the thin (14 and 37 nm) Co_2MnSi films is twice that of the thicker films, indicating that defect scattering is even more dominant in these films.

The saturation AH conductivity, derived from the data in figures 3(b) and (c) ($\sigma_{xy,\mathrm{sat}} = \rho_{xy,\mathrm{sat}}/\rho_{xx}^{-2}$), is plotted in figure 4. The magnitude of the AH conductivity decreases with decreasing thickness, but it remains relatively temperature independent in the thinner Co_2MnSi films with strongly temperature dependent saturation magnetization. In the thinner films, the reaction zone is largely comprised of island facets, rather than being a continuous layer, so whilst the volume of the reaction zone is similar to that of the Heusler layer, it may not provide a significant conduction path in transport measurements. The difference with the strongly temperature dependent AH conductivity of the NiMnSb film is striking.

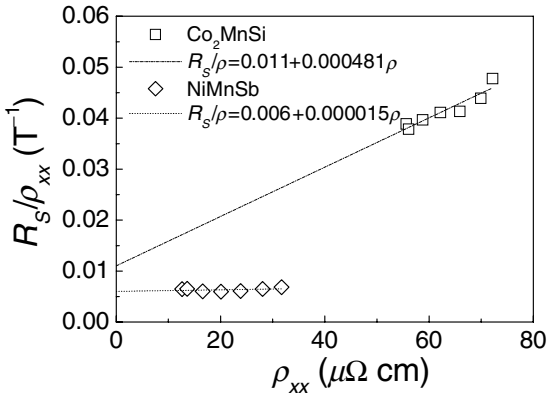

Figure 5. AH constant divided by resistivity versus resistivity, for the 260 nm Co_2MnSi:GaAs and 330 nm NiMnSb:GaAs films. Symbols represent data and dashed lines linear fit with the fit parameters shown in the figure caption.

As previously discussed, ρ_{xy} can vary in a complex manner with ρ_{xx} when the same physical processes are contributing to both terms. To determine the precise relationship between the resistivity and the Hall term it is customary to plot R_S/ρ_{xx} against ρ_{xx} where ($R_S = \rho_{xy,sat}/M_{sat}$). This is shown for the thick Co_2MnSi and NiMnSb films in figure 5, and an iterative linear fit is also shown for each sample. From this fitting it is clear that both samples can be described by the relationship $\rho_{xy} = \alpha\rho_{xx} + \beta\rho_{xx}^2$. The intercept, α, is positive, and of similar magnitude for the Co_2MnSi ($0.011\,T^{-1}$) and NiMnSb films ($0.006\,T^{-1}$). For NiMnSb the intercept dominates, because the slope, β, is negligible ($1.5 \times 10^{-5}(T\,\mu\Omega\,cm)^{-1}$), in contrast, for Co_2MnSi it is the slope ($4.81 \times 10^{-4}(T\,\mu\Omega\,cm)^{-1}$) that dominates R_S/ρ_{xx} in the accessible range of resistivities.

Recently, it was shown that mixed linear and quadratic dependence of ρ_{xy} on ρ_{xx} can arise in a purely extrinsic model when symmetric and asymmetric (spin-orbit) scattering occur [18]. By Matthiessen's rule one can describe the resistivity as arising from two components, $\rho_{xx} = \rho_0 + \rho_S$, where ρ_0 and ρ_S arise from symmetric and asymmetric skew scattering respectively. This model suggests that the observed behaviour for NiMnSb requires that both ρ_S and ρ_0 are variable functions of temperature and that both asymmetric and symmetric scatterers contribute significantly to the in-plane resistivity. A strong temperature dependence of the scattering terms is consistent with the claims of a crossover from half-metallic to ordinary ferromagnetic behaviour [36], with the onset of spin-flip scattering above 80 K in NiMnSb.

For the Co_2MnSi film, the predominantly quadratic relationship $\rho_{xy} \sim \beta\rho_{xx}^2$ shown in figure 5 can be interpreted as resulting from the same scattering mechanism dominating at all temperatures. We note that the results could also be accounted for in a purely intrinsic model, with robust P_t in Co_2MnSi, and a temperature dependent P_t in NiMnSb, but we rule out this scenario on physical grounds, as the resistivity ratio of the Co_2MnSi film (see table 1) is characteristic of 'dirty metal' with strong impurity scattering.

Thus as a result of this analysis, it is now clear that the temperature dependence of the AH conductivity when the extrinsic mechanism dominates (as is the case for all the films studied here) can only be used to measure the variation of the underlying polarization of the transport carriers in films when the scattering contributions to the resistivity are fully evaluated. A full analysis of the transport parameters, in particular, scattering processes and spin-orbit coupling parameters is required to employ AH conductivity as a measure of transport spin-polarization, but trends

observed in a systematically varied series can provide valuable information. As we have shown here for the NiMnSb film, a decreasing AH conductivity can result from competing scattering mechanisms and the behaviour might be rather subtle and may very well not reflect a declining P_t. For the Co_2MnSi it is difficult to imagine how a temperature independent ρ_{xy} could be observed in the presence of a declining P_t, although ρ_{xy} will also be sensitive to a temperature dependence of the spin-orbit coupling parameter, and it is possible although highly unlikely that these two terms counter-balance each other. The trend of decreasing AH conductivity with decreasing thickness in sputtered Co_2MnSi films is consistent with increasing spin-polarization as the distance from the interface increases and the manganese deficiency cause by the interface reaction decreases.

In summary, the sputtered Co_2MnSi films on GaAs (001) have large residual resistivities as a result of temperature independent defect scattering, which is the dominant scattering mechanism up to room temperature. This temperature independent extrinsic regime allows much more information about the spin-polarization to be extracted from the AH conductivity, which is sensitive to both spin-polarization and scattering mechanism, than is usually the case. We observe that the AH conductivity, and hence the spin-polarization, is robust up to room temperature in all the Co_2MnSi films, and its absolute value decreases as the thickness decreases and the loss of manganese into the interface reaction layer becomes more significant. This temperature independence in the Hall conductivity of the thinner films is surprising given the decreasing saturation magnetization. This may arise because the magnetization measurement is sensitive to the whole volume, whereas the transport only samples the conducting region, and the faceted morphology of the reaction zone in these films does not provide a good conduction path. The importance of the temperature independent extrinsic regime for the AH analysis is illustrated by comparison with an MBE grown NiMnSb film on GaAs (001) with low antisite disorder. The residual resistivity is far smaller in the NiMnSb film, there is less defect scattering, and there is a change in the dominant scattering mechanism between 10 K and room temperature. This particular difference is a result of the different growth methods, not of a difference between the materials. At all temperatures the ordinary Hall constant is far greater, and the AH constant far smaller than in the Co_2MnSi films, and it is quite strongly temperature dependent. Furthermore, the AH constant varies with the square of the resistivity in Co_2MnSi, whereas it is nearly linear in resistivity in the NiMnSb film. These observations indicate that the higher structural quality of the NiMnSb film results in a lower carrier density, higher mobility and reduced impurity scattering than in the 'dirty metal' Co_2MnSi films. The temperature dependent AH conductivity of the MBE grown NiMnSb could be attributed to either the changing scattering mechanism, or decreasing spin-polarization with increasing temperature.

Acknowledgments

This study was funded by the UK EPSRC; WRB is supported by the Ramsay Memorial Fellowships Trust.

References

[1] Ishida S, Fujii S, Kashiwagi S and Asano S 1995 *J. Phys. Soc. Japan* **64** 2152
[2] de Groot R A, Mueller F M, van Engen P G and Buschow K H J 1983 *Phys. Rev. Lett.* **50** 2024
[3] Brown P J, Neumann K U, Webster P J and Ziebeck K R A 2000 *J. Phys.: Condens. Matter* **12** 1827

[4] Wurmehl S, Fecher G H, Kandpal H C, Ksenofontov V, Felser C, Lin H J and Morais J 2005 *Phys. Rev.* B **72** 184434
[5] Bach P *et al* 2003 *Appl. Phys. Lett.* **83** 521
[6] Webster P J 1971 *J. Phys. Chem. Solids* **32** 1221
[7] Orgassa D, Fujiwara H, Schulthess T C and Butler W H 1999 *Phys. Rev.* B **60** 13237
[8] Picozzi S, Continenza A and Freeman A J 2004 *J. Magn. Magn. Mater.* **272–76** 315
[9] Picozzi S, Continenza A and Freeman A J 2004 *Phys. Rev.* B **69** 094423
[10] Hurd C M 1972 *The Hall Effect in Metals and Alloys* (New York: Plenum)
[11] Hirsch J E 1999 *Phys. Rev. Lett.* **83** 1834
[12] Sinova J, Culcer D, Niu Q, Sinitsyn N A, Jungwirth T and MacDonald A H 2004 *Phys. Rev. Lett.* **92** 126603
[13] Kato Y K, Myers R C, Gossard A C and Awschalom D D 2004 *Science* **306** 1910
[14] Wunderlich J, Kaestner B, Sinova J and Jungwirth T 2005 *Phys. Rev. Lett.* **94** 047204
[15] Sih V, Myers R C, Kato Y K, Lau W H, Gossard A C and Awschalom D D 2005 *Nat. Phys.* **1** 31
[16] Nozieres P and Lewiner C 1973 *J. Phys.* **34** 901
[17] Lee W L, Watauchi S, Miller V L, Cava R J and Ong N P 2004 *Science* **303** 1647
[18] Gerber A, Milner A, Finkler A, Karpovski M, Goldsmith L, Tuaillon-Combes J, Boisron O, Melinon P and Perez A 2004 *Phys. Rev.* B **69** 224403
[19] Berger L 1970 *Bull. Am. Phys. Soc.* **15** 266
[20] Otto M J, Vanwoerden R A M, Vandervalk P J, Wijngaard J, Vanbruggen C F and Haas C 1989 *J. Phys.: Condens. Matter* **1** 2351
[21] Nadgorny B, Mazin I I, Osofsky M, Soulen R J, Broussard P, Stroud R M, Singh D J, Harris V G, Arsenov A and Mukovskii Y 2001 *Phys. Rev.* B **63** 184433
[22] Singh L J, Barber Z H, Miyoshi Y, Bugoslavsky Y, Branford W R and Cohen L F 2004 *Appl. Phys. Lett.* **84** 2367
[23] Singh L J, Barber Z H, Miyoshi Y, Branford W R and Cohen L F 2004 *J. Appl. Phys.* **95** 7231
[24] Singh L J, Barber Z H, Kohn A, Petford-Long A K, Miyoshi Y, Bugoslavsky Y and Cohen L F 2006 *J. Appl. Phys.* **99** 013904
[25] Sakuraba Y, Nakata J, Oogane M, Kubota H, Ando Y, Sakuma A and Miyazaki T 2005 *Japan. J. Appl. Phys.* **44** L1100
[26] Dong X Y, Adelmann C, Xie J Q, Palmstrom C J, Lou X, Strand J, Crowell P A, Barnes J P and Petford-Long A K 2005 *Appl. Phys. Lett.* **86** 102107
[27] Manyala N, Sidis Y, Ditusa J F, Aeppli G, Young D P and Fisk Z 2004 *Nat. Mater.* **3** 255
[28] Branford W R *et al* 2004 *Phys. Rev.* B **69** 201305(R)
[29] Ishida S, Masaki T, Fujii S and Asano S 1998 *Physica* B **245** 1
[30] Van Roy W, De Boeck J, Brijs B and Borghs G 2000 *Appl. Phys. Lett.* **77** 4190
[31] Wojcik M, Van Roy W, Jedryka E, Nadolski S, Borghs G and De Boeck J 2002 *J. Magn. Magn. Mater.* **240** 414
[32] Ravel B, Raphael M P, Harris V G and Huang Q 2002 *Phys. Rev.* B **65** 184431
[33] Petford-Long A K, Kohn A, Bromwich T, Jackson V, Castano F and Singh L J 2006 *Thin Solid Films* **505** 10
[34] Otto M J, Vanwoerden R A M, Vandervalk P J, Wijngaard J, Vanbruggen C F, Haas C and Buschow K H J 1989 *J. Phys.: Condens. Matter* **1** 2341
[35] Branford W R, Roy S B, Clowes S K, Miyoshi Y, Bugoslavsky Y V, Gardelis S, Giapintzakis J and Cohen L F 2004 *J. Magn. Magn. Mater.* **272–276** E1399
[36] Hordequin C, Ristoiu D, Ranno L and Pierre J 2000 *Eur. Phys. J.* B **16** 287